RSC
Applied Interfaces

Accepted Manuscript

This article can be cited before page numbers have been issued, to do this please use: G. Marchiori, R. Seraglia, G. A. Rizzi, C. Maccato, M. Benedet, E. Callone, S. Dirè, A. Gasparotto and D. Barreca, *RSC Appl. Interfaces*, 2024, DOI: 10.1039/D4LF00259H.

ROYAL SOCIETY OF CHEMISTRY

rsc.li/RSCApplInter

RSC Applied Interfaces

View Article Online
DOI: 10.1039/D4LF00259H

ARTICLE

On defect-engineered graphitic carbon nitride on carbon cloth supports for the photoelectrocatalytic degradation of organophosphate pesticides

Giacomo Marchiori,[a] Roberta Seraglia,[b] Gian Andrea Rizzi,[a,b] Chiara Maccato,[a,b,*] Mattia Benedet,[a,b] Emanuela Callone,[c] Sandra Dirè,[c] Alberto Gasparotto,[a,b] and Davide Barreca[b]

The effective degradation of persistent aqueous pollutants, such as Fenitrothion (FNT), a widely used organophosphate pesticide, represents a major urgency for the protection of human health and environment. In this regard, this study is focused on the fabrication of green photoelectrocatalysts based on graphitic carbon nitride (gCN), capable of generating hydrogen peroxide (H_2O_2) to trigger electro-Fenton processes for FNT degradation. In particular, electrophoretic deposition of gCN onto carbon cloth (CC) substrates was performed starting from gCN powders designed *via* thermal condensation of urea mixed with acetylacetone (AcAc). The resulting defect engineering promoted an improved gCN light harvesting capability and an enhanced separation of photogenerated charge carriers. The obtained supported materials featured an attractive electrochemical reactivity and operational stability, opening the door to their possible real-world end-use. The present work illustrates, as a proof-of-concept, the potential of gCN-based photoelectrocatalysts in water treatment technologies, offering a sustainable solution in a greener perspective to mitigate the environmental impact of hazardous pollutants.

Received 00th January 20xx,
Accepted 00th January 20xx

DOI: 10.1039/x0xx00000x

1. Introduction

The presence in the environment and in water of organophosphate compounds, widely used in agriculture as pesticides, has raised a significant concern due to their harmful effects on animal and human health even at trace levels.[1, 2] These issues, along with their persistence against the most common treatments, have stimulated extensive efforts aimed at the development of methods enabling their efficient monitoring and removal.[3, 4] To this aim, an attractive solution is provided by advanced oxidation processes (AOPs),[5] that are based on the generation of reactive oxygen species (ROS, among which •OH) promoting the oxidative decontamination of polluted aqueous solutions. Among the most successful AOPs, electro-Fenton (EF) routes offer various concurrent advantages for the degradation of numerous organic contaminants, encompassing fertilizers, pesticides, dyes, surfactants, and drugs' active ingredients.[6]

In view of real-world applications of EF processes, the development of low cost, abundant, highly active and metal-free catalysts is highly required,[7] since systems based on precious metals have a high environmental impact and also suffer from low selectivity and durability.[8] In this regard, an appealing alternative is offered by 2D materials and, in particular, by graphitic carbon nitride (gCN; $E_G \approx$ 2.7 eV). The latter, a low-cost semiconductor comprising naturally abundant elements, is a rising star in the field of photo(electro)catalysis thanks to the non-toxicity, the capability of absorbing Vis radiation, and the broad variability of morphological, structural, and electronic properties.[9] In fact, the chemico-physical characteristics of gCN-based materials are directly dependent on the adopted synthetic routes, usually involving thermal condensation of N-containing organic precursors (such as urea, melamine, cyanamide and thiourea).[9] Various studies have so far been focused on gCN photo(electro)catalysts for water and air purification, CO_2 reduction, H_2O_2 production, and water splitting,[10-14] but, to our knowledge, the use of gCN photoelectrocatalysts for FNT degradation has never been reported up to date.

In the present work, gCN was used to develop photocathodes for the efficient generation of H_2O_2 to foster EF processes for the degradation of FNT, an aromatic organophosphate pesticide.[15] The target systems were synthesized starting from the sole urea, and from urea mixed with AcAc. The functionalization with AcAc was aimed at graphitic carbon nitride defect engineering,[16, 17] in order to favourably boost the resulting photoelectrocatalytic activity. The corresponding powdered materials were used as precursors for the preparation of supported photoelectrocatalysts *via* electrophoretic deposition (EPD) (Scheme 1), an amenable route utilized in our research group to fabricate a variety of gCN-based electrocatalysts for the oxygen evolution reaction (OER).[18-20] The target systems were grown on flexible CC substrates, ensuring an excellent electrical conductivity and good corrosion resistance.[21] To assess the influence of AcAc introduction on the system properties, both chemico-physical characterization and functional (photo)electrochemical tests were carried out on both the gCN containing AcAc, and the bare gCN obtained by urea as such. The monitoring of FNT degradation during EF experiments was performed by high performance liquid chromatography-mass spectrometry (HPLC-MS), analysing the

[a] Department of Chemical Sciences – Padova University and INSTM, Via Marzolo, 1 - 35131 Padova, Italy * E-mail: chiara.maccato@unipd.it.
[b] CNR-ICMATE and INSTM – Department of Chemical Sciences – Padova University, Via Marzolo 1, and Corso Stati Uniti 4 – 35127 Padova, Italy
[c] "Klaus Müller" Magnetic Resonance Laboratory, Department of Industrial Engineering – Trento University, Via Sommarive, 9 - 38123 Trento, Italy
† Electronic Supplementary Information (ESI) available. See DOI: 10.1039/x0xx00000x

View Article Online
DOI: 10.1039/D4LF00259H

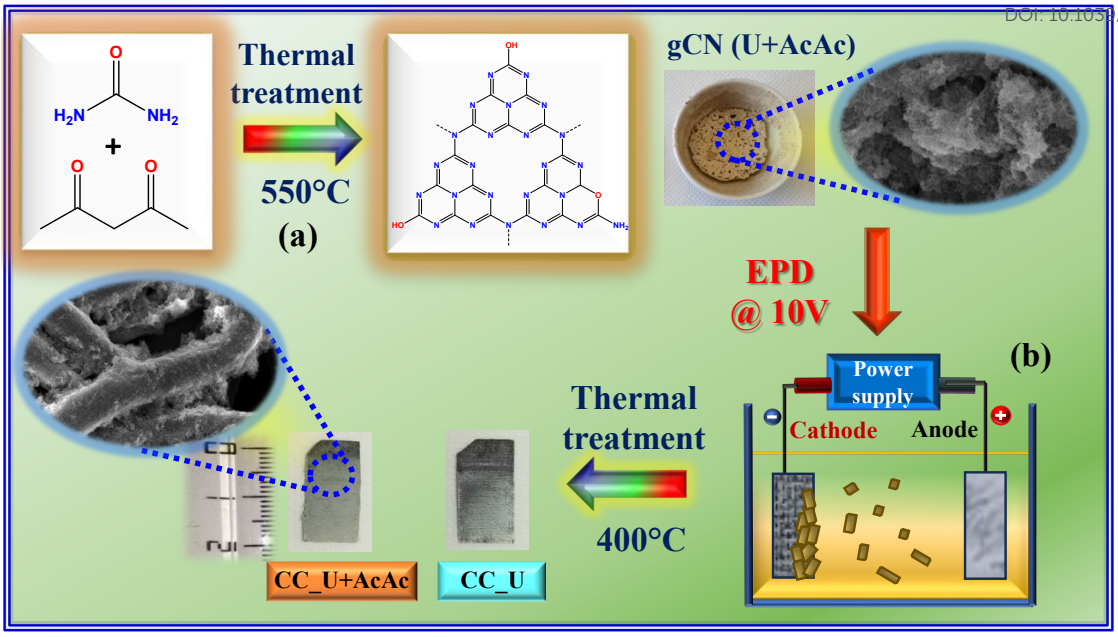

Scheme 1. Sketch of the procedure adopted in the present work for (a) the thermal synthesis of gCN powders and (b) the subsequent preparation of gCN-containing electrode materials. U = urea; AcAc = acetylacetone; CC = carbon cloth; EPD = electrophoretic deposition. The suspensions for EPD were prepared by dispersing 40 mg of finely grinded carbon nitride powders into a beaker containing 50 mL of acetone and 4 mg of freshly dissolved I_2 (Sigma-Aldrich, ≥ 99.8 %), followed by sonication for 30 min. For more details on the experimental procedures, see ESI†, § S1.

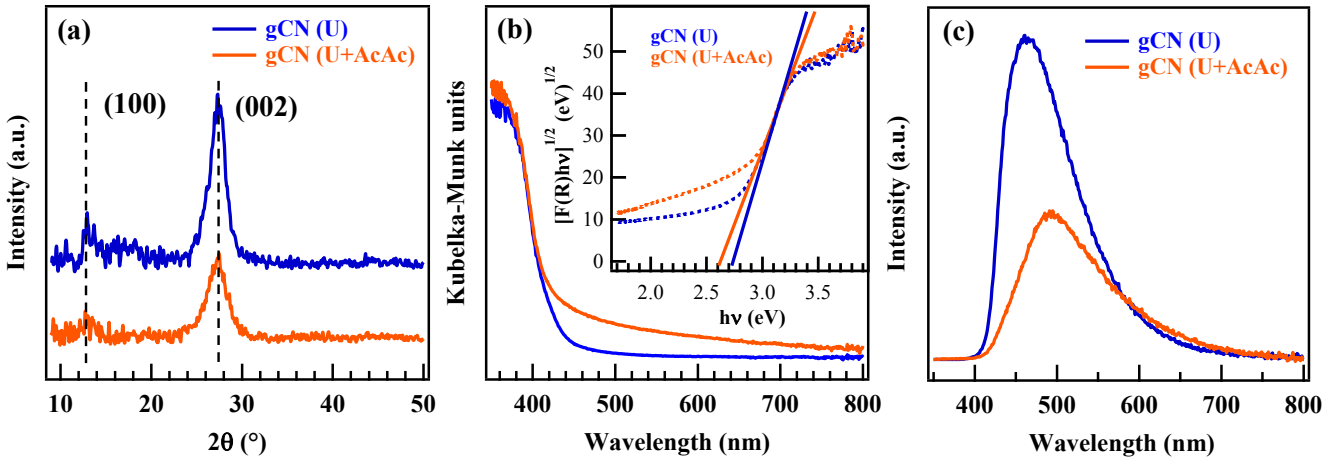

Fig. 1 Physico-chemical characterization of gCN (U) and gCN (U+AcAc) powders: (a) XRD patterns; (b) UV-Vis spectra and (inset) Tauc plots; (c) PL spectra.

working solutions as a function of time during degradation experiments. In the following, particular emphasis is given to the interrelations between material structure, composition, morphology, optical properties, and functional performances.

2. Experimental

2.1 Synthesis

gCN precursor powders were synthesized following previous works,[16, 17] and performing a subsequent optimization of the thermal treatment conditions. Deposition onto CC substrates was carried out *via* EPD under previously reported conditions[18, 22] (see also ESI†, §S1). Henceforth, powders obtained from the sole urea and from urea and acetylacetone will be referred to as gCN (U) and gCN (U+AcAc), whereas the corresponding CC-supported specimens will be denoted as CC_U and CC_U+AcAc, respectively.

2.2 Characterization

X-ray diffraction (XRD) measurements were collected using a Bruker AXS D8 Advance Plus diffractometer, equipped with a Cu Kα X-ray source (λ = 1.54 Å). The average crystal size was estimated through the Scherrer equation. Analyses were performed at the PanLab facility (Department of Chemical Sciences, Padova University) founded by MIUR Dipartimento di Eccellenza grant "NExuS". Fourier transform-infrared (FT-IR) diffuse reflectance spectra were recorded by diluting gCN within dried KBr powders, using a Jasco FT/IR-4100 instrument (resolution = 4 cm^{-1}). UV-Vis diffuse reflectance and photoluminescence (PL) spectra were acquired on a FLS1000 (Edinburgh Instruments) spectrophotometer (excitation wavelength

= 330 nm; spectral bandwidth = 1 nm). Band gap (E_G) values were estimated using the Tauc equation – plots of $[F(R)hv]^n$ vs. hv, where F(R) is the Kubelka–Munk function, hv is the photon energy, and R is the measured reflectance, assuming indirect and allowed transitions (n = 1/2).[23] ^{13}C and ^{15}N solid state nuclear magnetic resonance (NMR) analyses were carried out with a Bruker Avance 400WB spectrometer with a CPMAS double-band 4 mm probe (ESI†, § S.2).

X-ray photoelectron spectroscopy (XPS) analysis was performed using an ESCALAB™ QXi spectrometer funded by "Sviluppo delle infrastrutture e programma biennale degli interventi del Consiglio Nazionale delle Ricerche (2019)", at a working pressure of ≈ 5×10^{-9} mbar, using a monochromatized Al Kα X-ray source ($h\nu$ = 1486.6 eV). Binding energy (BE) values were corrected for charging by assigning a value of 284.8 eV to the adventitious C1s component. Atomic percentages (at. %) were calculated by peak area integration, using ThermoFisher sensitivity factors. Peak fitting was carried out by XPSPEAK (Version 4.1) software,[24] using Gaussian-Lorentzian sum functions. Field emission scanning electron microscopy (FE-SEM) analyses were carried out using a Zeiss SUPRA 40VP instrument, at primary beam acceleration voltages between 5 and 20 kV. Photoelectrochemical and electro-Fenton degradation tests were conducted by employing the prepared supported materials as working electrodes in 0.1 M Na_2SO_4 aqueous solution, in a three-electrode configuration (see also Fig. S1†). A HPLC-MS apparatus, equipped with an electrospray ionization (ESI) ion source, was employed to monitor FNT degradation. Further data on characterization and functional tests are reported in the ESI† (§S2).

3. Results and discussion

In this work, attention was first dedicated to the FT-IR characterization of the starting powders, revealing the occurrence of carbon nitride-based materials containing an appreciable amount of -NH_x (x = 1, 2) and -OH groups (see also Fig. S2†, Table S1† and ESI†, page S8-S9). Accordingly, the powders XRD patterns (Fig. 1a) were dominated by a peak at 2θ = 27.5° attributed to the interplanar (002) stacking of gCN sheets, whereas the low-intensity signal at 2θ = 13.1° was ascribed to the periodic arrangement of tri-*s*-triazine units in (100) crystallographic planes.[25-28] According to the Scherrer equation, both samples featured an average crystallite size of ≈ 5 nm, irrespective of preparative conditions. The lower intensity of both signals in gCN (U+AcAc) sample can be attributed to AcAc functionalization, resulting in a higher content of defects responsible, in turn, for a decreased crystallinity.[16, 17]

Optical absorption spectra (Fig. 1b) were dominated by a strong absorption at λ < 440 nm, associated to gCN interband electronic transitions.[25, 27, 28] Differently from gCN (U), gCN (U+AcAc) also displayed a moderate, but well detectable, absorption at λ > 440 nm, that can be ascribed to inter-band states due to AcAc functionalization , associated to defect formation (see also XPS data below).[16, 17] The extrapolated E_G values (Fig. 1b, inset) were 2.74 and 2.62 eV for gCN (U) and gCN (U+AcAc), respectively, confirming a broadened optical absorption for the latter system,[16, 17] a favourable issue for an improved Vis-light exploitation. PL spectra (Fig. 1c) displayed a strong fluorescence emission, centred at ≈ 470 and 500 nm for gCN (U) and gCN (U+AcAc), respectively, due to the radiative relaxation of excited electrons from the conduction to the valence band.[25-28] The red shift of the emission maximum could be related to the lower gCN (U+AcAc) band gap, as previously discussed. The lowered PL intensity in the case of gCN (U+AcAc) proved that AcAc functionalization was effective in suppressing charge carriers' recombination, a beneficial feature in view of the target end use (see also below).

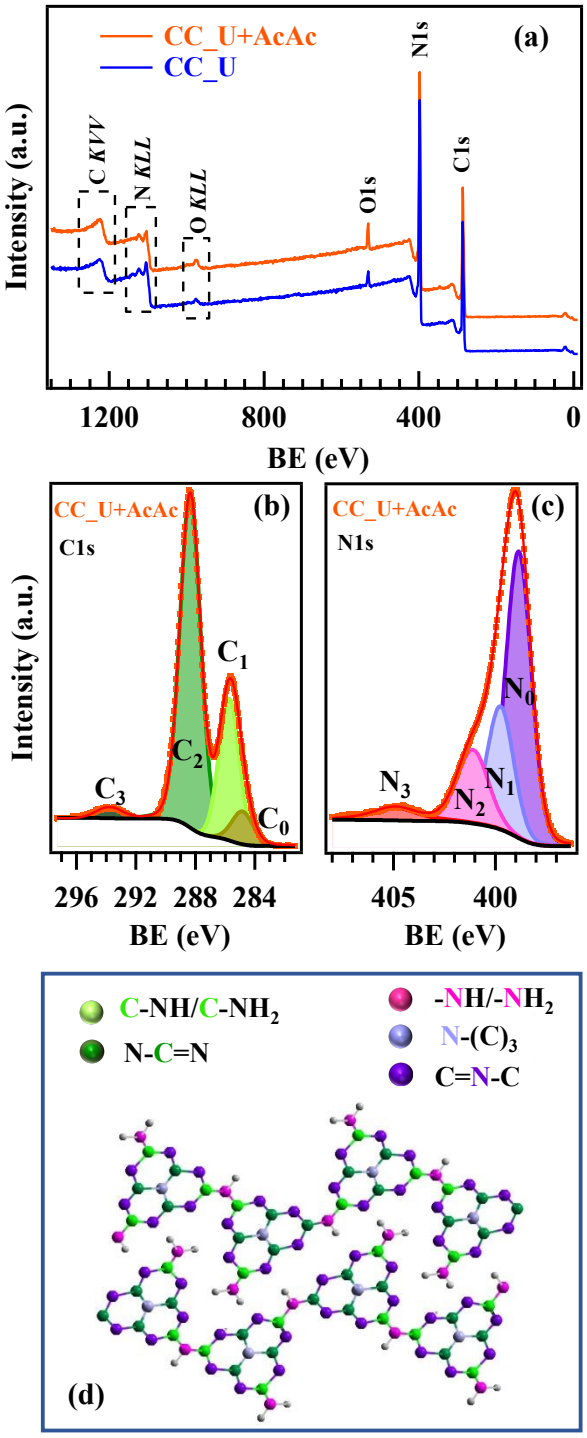

Fig. 2 (a) XPS survey of CC_U and CC_U+AcAc samples. (b) C1s and (c) N1s photoelectron peaks for CC_U+AcAc. (d) Sketch of gCN structure[18, 23]: colour codes identifying non-equivalent C and N atoms are the same used for the different C1s and N1s fitting components.

Material composition was preliminarily investigated by nuclear

View Article Online DOI: 10.1039/D4LF00259H

magnetic resonance (NMR) (ESI†, §S3.2 and Fig. S3†), that supported the formation of tris-*s*-triazine units in gCN.[29] ^{13}C cross polarization/magic angle spinning (CPMAS) spectra of both samples presented two resonances at 165 and 157 ppm, attributable respectively to C-NH_x, and to [N-C=N] moieties in a ≈1: 1 ratio, as revealed by quantitative ^{13}C MAS experiments. It is worth mentioning that C-NH_x resonance can be satisfactory fitted with two components, whose ratio changes between the two samples suggesting different amounts of C-NH_2 and C-NH-C defects (Table S2, ESI†). The ^{15}N CPMAS spectra presented four resonances centred at ≈195, 157, 136 and 117 ppm due to C-N=C, N-C_3, -NH- and -NH_2 groups,[29] respectively, with small lineshape differences, in agreement with ^{13}C results and other spectroscopic data.

Important complementary information was provided by XPS. Wide scan spectra (Fig. 2a) highlighted the presence of only C, N, and O. C1s signals (Fig. 2b and S4a†) were decomposed by four components: **C_0**, attributed to both adventitious carbon and the CC substrate;[30, 31] **C_1**, due to both terminal C-NH_x (x = 1, 2) moieties[20, 22, 23, 32] and C-O groups;[17, 31] **C_2**, the most intense band, assigned to C atoms in N-C=N moieties;[19, 20, 33] **C_3**, related to π electronic excitations.[34, 35] For the AcAc-functionalized specimen, **C_1** contribution turned out to be higher (Table S3†), demonstrating that AcAc functionalization resulted in a higher content of defective sites, since these amino-groups should not be present in a fully condensed gCN structure. This conclusion was in line with the analysis of N1s photopeaks, which resulted from the contribution of four bands (Fig. 2c and Fig. S4b†): **N_0**, the main one, due to bi-coordinated N centres (C=N-C);[17, 19, 20, 22] **N_1**, corresponding to N-$(C)_3$ nitrogen atoms in gCN;[17, 19, 32, 33] **N_2**, related to uncondensed -NH_x groups[19, 20] **N_3**, due to π electronic excitations.[36, 37] The higher relative weight of **N_2** in CC_U+AcAc with respect to CC_U (Table S4†) indicated a higher content of defects resulting from -NH_x presence, that can act as capturing sites, minimizing charge carrier recombination and enhancing the system photoactivity,[23] as confirmed by PL analyses.[17, 34, 38] Further details are reported in the ESI† (§S4; Fig. S5†-S7† and Tables S5-S6†). Overall, XPS results highlighted that CC_U+AcAc, possessed a higher content of uncondensed -NH_x and -OH groups coordinated to nitrogen defects. These results prove that AcAc functionalization is a viable tool to achieve carbon nitride defect engineering.

FE-SEM analyses evidenced that bare CC (Fig. 3a) was characterized by the presence of interwoven fibres (average diameter ≈10 µm), whose assembly resulted in a network with an open morphology. For both CC_U and CC_U+AcAc (Fig. 3b-c), gCN deposition, yielding aggregates with a sheet-like morphology, resulted in an increase of the overall active area. The latter feature favourably affects catalytic activity thanks to: i) a higher density of surface active sites; ii) an enhanced injection of photogenerated

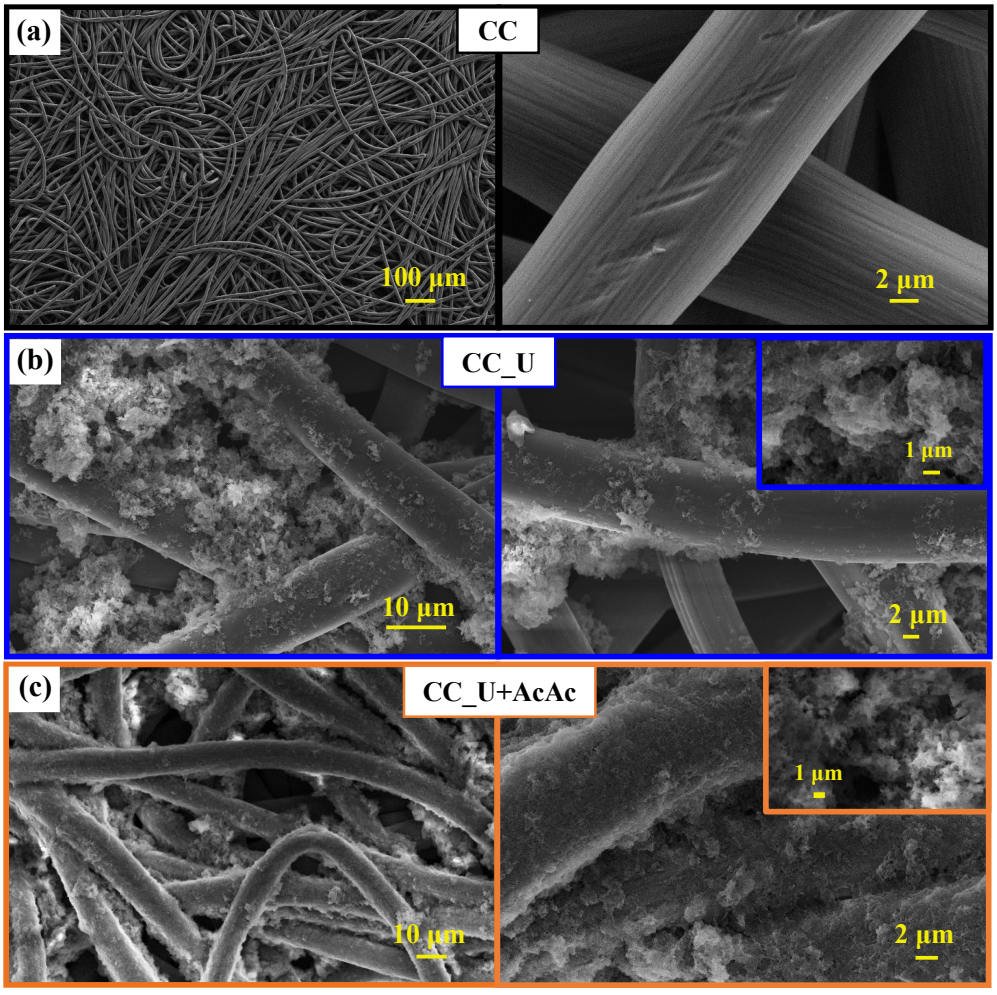

Fig. 3 Representative FE-SEM micrographs for: (a) bare carbon cloth; (b) CC_U sample; (c) CC_U+AcAc sample.

charge carries into the electrolyte, suppressing detrimental recombination.[18, 25-28] A detailed micrograph inspection revealed that, for CC_U (Fig. 3b), gCN particles were aggregated in confined areas, leaving uncovered various CC regions. Conversely, a more homogeneous carbon nitride dispersion was observed for CC_U+AcAc (Fig. 3c), for which gCN aggregates 'welded' in some cases the spaces between contiguous fibres, penetrating into the cloth meshes. Such a difference can be rationalized basing on the above results. In fact, the powder attachment to the CC substrate likely occurs through the establishment of bonds involving terminal -NH_x and -OH groups, a process promoted by the annealing treatment.[39] In fact, the larger amount of uncondensed amino groups, observed for gCN (U+AcAc), favoured a better deposit adhesion to the underlying CC. This result underscores another important advantage brought about by defect engineering resulting from AcAc functionalization.

Overall, the characterization results reported so far suggest that carbon nitride flakes in gCN (U+AcAc) are internally less condensed (and, hence, more amino-rich), than in gCN (U). As discussed below, this result might explain the better catalytic activity of the electrode material prepared by gCN (U+AcAc) powders towards the $O_2 \rightarrow H_2O_2$ reduction reaction. In fact, although the exact nature and behaviour of the various gCN defects' types is still a matter of debate, -NH_x groups have been reported to promote charge separation (acting as trapping agent for holes) and interfacial electron transfer. In addition, their Lewis basicity is also beneficial to the photoreduction reaction, thus positively impacting on material functional performances.[40, 41]

Prior to FNT degradation tests, photoelectrochemical characterization was carried out by employing gCN materials as working electrodes (Fig. 4a). Cyclic voltammetries (CV, Fig. S8†) showed two significant reduction peaks at more positive potential values than H_2 evolution: the first one, attributed to 2e$^-$ oxygen reduction reaction (ORR) yielding the formation of H_2O_2 from O_2; the second one, associated to the $H_2O_2 \rightarrow H_2O$ reduction and the direct 4e$^-$ ORR resulting in the formation of H_2O from O_2 (see ESI†, page S16).[42] The reduction peaks were also evident in linear sweep voltammetries (LSV), showing that, under illumination, the signal for the 2e$^-$ ORR was shifted towards a more positive bias (Fig. 4b-c). The corresponding shift values (≈ 30 and ≈ 50 mV for CC_U and CC_U+AcAc) demonstrated that AcAc functionalization yielded an improvement in the system behaviour. Chronoamperometry (CA) measurements under the same conditions used for EF tests (Fig. 4d) did not reveal any significant current density decrease *vs*. time, a result highlighting the appreciable electrocatalyst stability, an important prerequisite for eventual real-world applications.

The attention was subsequently dedicated to EF experiments. As sketched in Fig. 5a, O_2 is reduced through a 2e$^-$ mechanism, leading to the formation of H_2O_2 "activated" by the Fenton cycle[6, 43] generating, in turn, $HO_2^\bullet$ and especially $^\bullet OH$, capable of boosting FNT degradation:

$$Fe^{2+} + H_2O_2 + H^+ \rightarrow Fe^{3+} + H_2O + {}^\bullet OH \quad (E° = 1.65\ V) \qquad (1)$$

$$Fe^{3+} + H_2O_2 \rightarrow Fe^{2+} + HO_2^\bullet + H^+ \quad (E° = 2.80\ V) \qquad (2)$$

As an alternative to (2), Fe^{3+} reduction can be promoted by $HO_2^\bullet$ (3) or by electron transfer at the surface (4):[6, 43]

$$Fe^{3+} + HO_2^\bullet \rightarrow Fe^{2+} + O_2 + H^+ \qquad (3)$$

$$Fe^{3+} + e^- \rightarrow Fe^{2+} \qquad (4)$$

Mass spectrometry measurements, in accordance with the literature,[44, 45] allowed to identify four different species, beside FNT, present in the working solution even before the real beginning of EF experiments (Fig. 5b). The occurrence of these compounds was associated to the acidification of the solution itself, which could have led to their formation from the pristine FNT through partial oxidation and hydrolysis processes. Fig. 5b presents the possible FNT degradation pathways taking place under the presently adopted conditions. After the start of EF tests, the newly generated ROS promoted the degradation of the indicated organic species, likely following similar reaction pathways. It is worth highlighting that, even if 3-methyl-4-nitrophenol (MW = 153) was the lowest molecular weight product among the identified ones, subsequent oxidative processes could produce even lighter organic species, undetectable via HPLC-MS measurements, due to their low concentrations and/or very short lifetimes in solution.

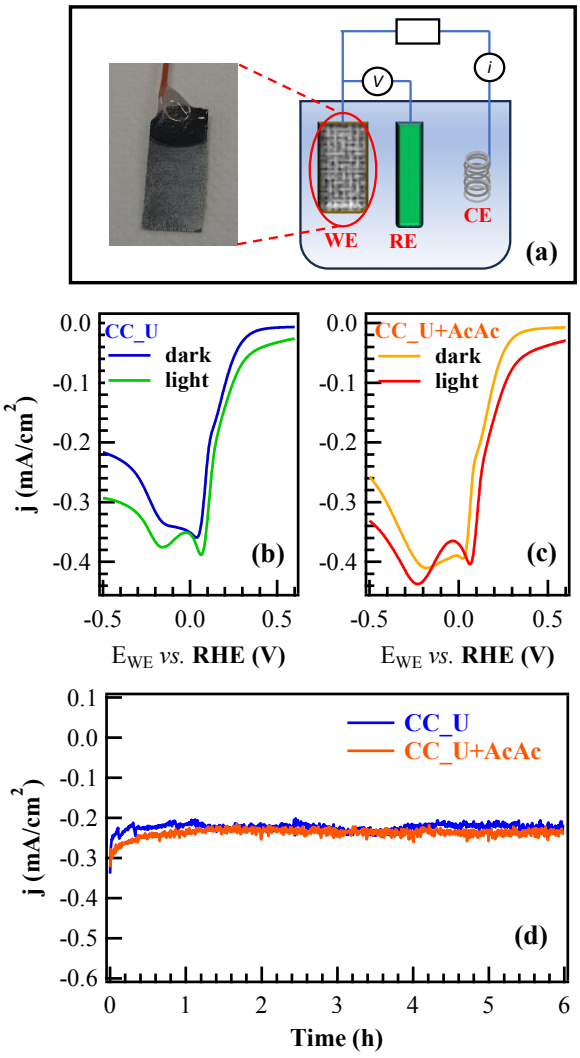

Fig. 4 (a) Diagram of the cell used for electrochemical tests (WE = working electrode; RE = reference electrode; CE = counter-electrode). (b,c) LSV in the dark and under illumination for CC_U and CC_U+AcAc. (d) CA curves recorded at a bias of +0.06 V *vs*. the reversible hydrogen electrode (RHE).

The relative concentration *vs*. time trends of the identified species are shown in Fig. 6a-b. Unexpectedly, FNT was never detected by HPLC-MS analysis, not even in the solution portions corresponding to time "0", at variance with the blank degradation test (Fig. S9†). This result was ascribed to the initial adsorption of FNT molecules onto the photoelectrocatalysts surface, removing an appreciable pesticide amount from the working solution. In fact, adsorbed FNT can likely be partially degraded directly onto the electrodes, yielding thus the other species found in the liquid phase.

The trends of FNT-derived species in EF tests are significantly different compared to the corresponding ones in the blank degradation experiment (see Fig. S9†), during which the relative

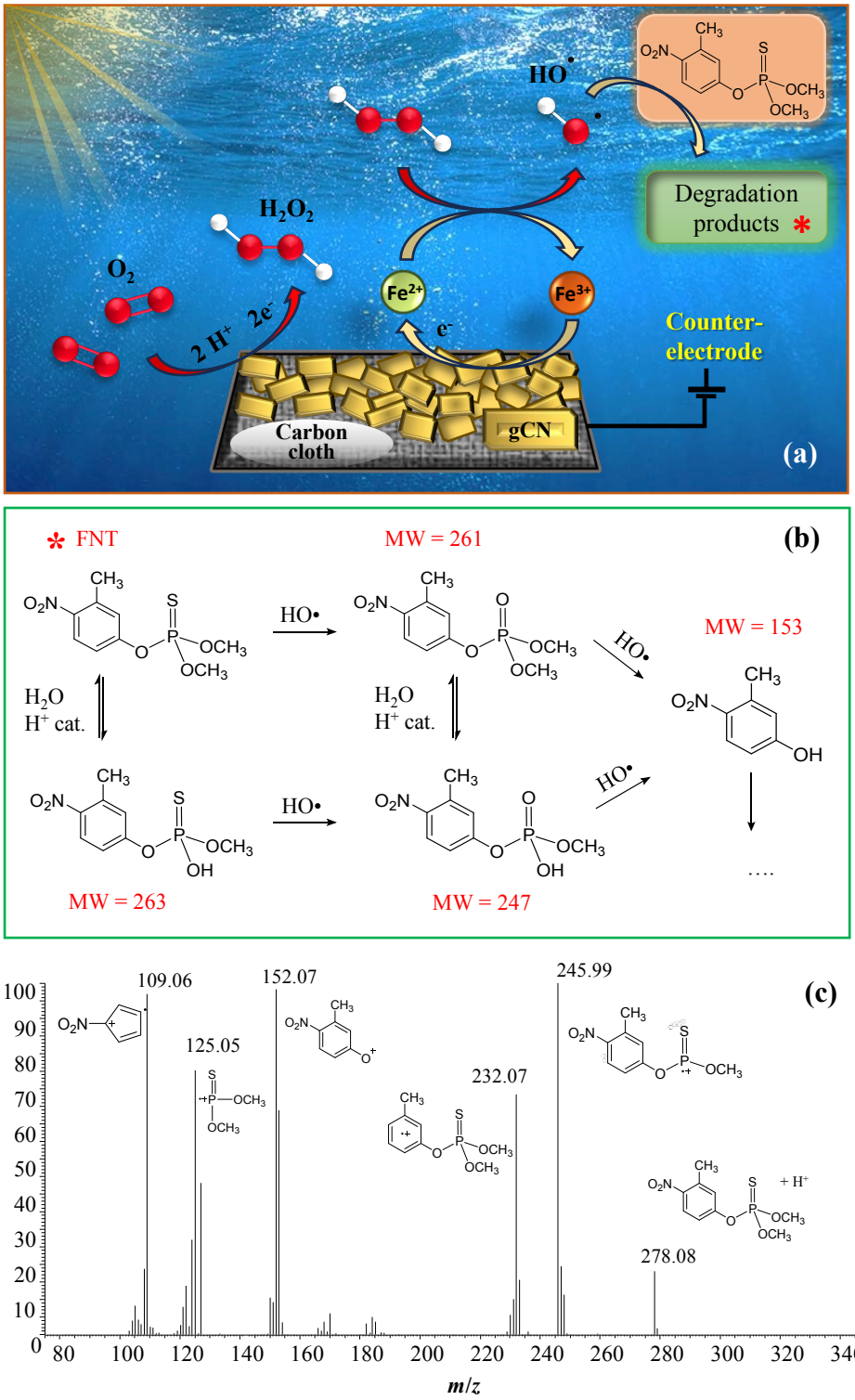

Fig. 5 (a) Sketch of the reactions involved in electro-Fenton process for FNT degradation. (b) Possible FNT degradation pathways and labelling of the species found in solution under the adopted conditions (MW = molecular weight). (c) Representative ESI-MS^2 fragmentation spectrum for FNT.

View Article Online
DOI: 10.1039/D4LF00259H

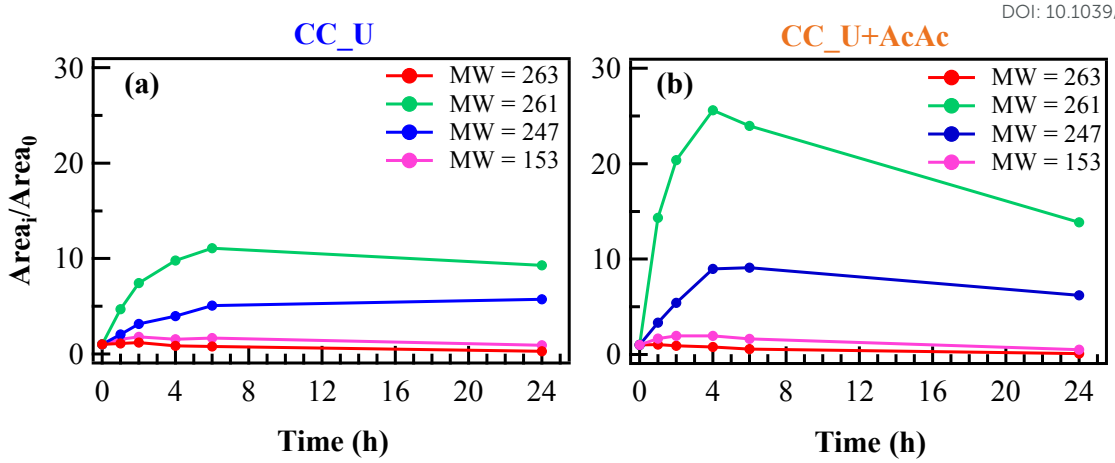

Fig. 6 Evolution of FNT degradation products during electro-Fenton experiments, using CC_U (a) and CC_U+AcAc (b) as working electrodes. For all species, the Area$_i$/Area$_0$ ratio was calculated as the ratio between the chromatographic peak area at the i-th time and at time = 0 h.

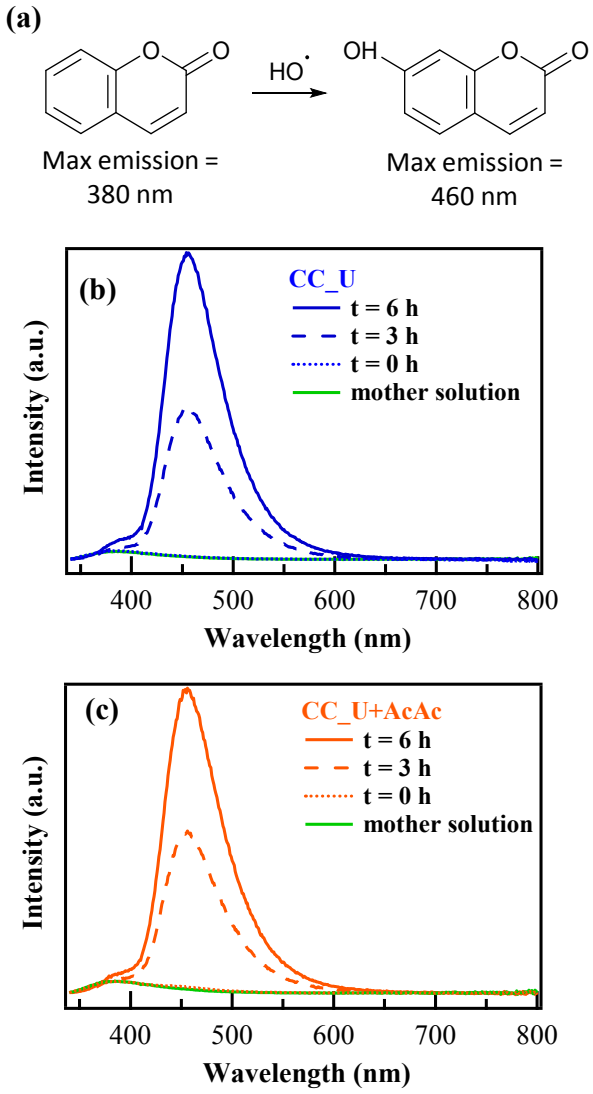

Fig. 7 (a) Oxidation of coumarin to 7-hydroxycoumarin. (b,c) Emission spectra of 1 mM coumarin solutions as a function of time using respectively CC_U and CC_U+AcAc as photocathodes in electro-Fenton experiments.

concentrations remained almost constant for 24 h. Notably, in EF tests the relative concentrations of species with MW =247 and 261 (see Fig. 5b and Fig. 6a-6b) underwent an increase during the first hours, more significant in the case of CC_U+AcAc. Correspondingly, a subsequent concentration decrease for these species was observed till the end of the test, demonstrating once again the beneficial role of defect engineering through AcAc functionalization. For comparison, results pertaining to FNT degradation on bare CC are reported in Fig. S10†.

In order to confirm the generation of H_2O_2 and oxidizing radical species *via* EF, further experiments were performed in solutions of coumarin (1-benzopyran-2-one), used due to its ability to act as a scavenger for •OH radicals.[46] In the presence of the latter, coumarin can be converted into 7-hydroxycoumarin (7-OHC), featuring a very intense fluorescence emission at $\lambda \approx 460$ nm, well distinct from the coumarin emission maximum at $\lambda \approx 380$ nm (Fig. 7a). The direct monitoring of 7-OHC formation provides a qualitative indication on the presence of •OH,[46] otherwise elusive due to their high reactivity and short lifetimes in solution ($\approx 10^{-9}$ s). Coumarin tests on both CC_U and CC_U+AcAc (Fig. 7b-c) resulted in the appearance of a strong emission signal at 460 nm at 3 and 6 h, absent for the mother solution and the samples at time "0". As stated above, this signal demonstrates the effective generation of •OH radicals in solution. It is also worth noting that, during EF tests conducted on FNT and coumarin, the formation of a well-adherent deposit on the working electrodes (Fig. 8a) took place (see also the pertaining characterization in the ESI†, Fig. S11†-S16† and Tables S7-S10†). Its dark orange colour suggested the formation of insoluble Fe(III) compounds, that was indeed confirmed by XPS analyses (see also ESI†, §S5.3). At variance with fresh samples (Fig. 2a), survey spectra (Fig. S11†) showed the presence of Na, Fe, S and P. Whereas Na and S occurrence (Fig. S12†) could be traced back to the used Na_2SO_4 electrolyte, P signals (Fig. S13†) arose from FNT decomposition products. Fe2p signal shape and positions [Fig. 8c; BE(Fe2p$_{3/2}$) = 711.7 eV] were in line with literature data for FeOOH,[47] whose formation could result from the continuous H^+ consumption during EF processes ($2e^-$ and $4e^-$ ORR, ESI†, page S16), causing a pH increase

View Article Online
DOI: 10.1039/D4LF00259H

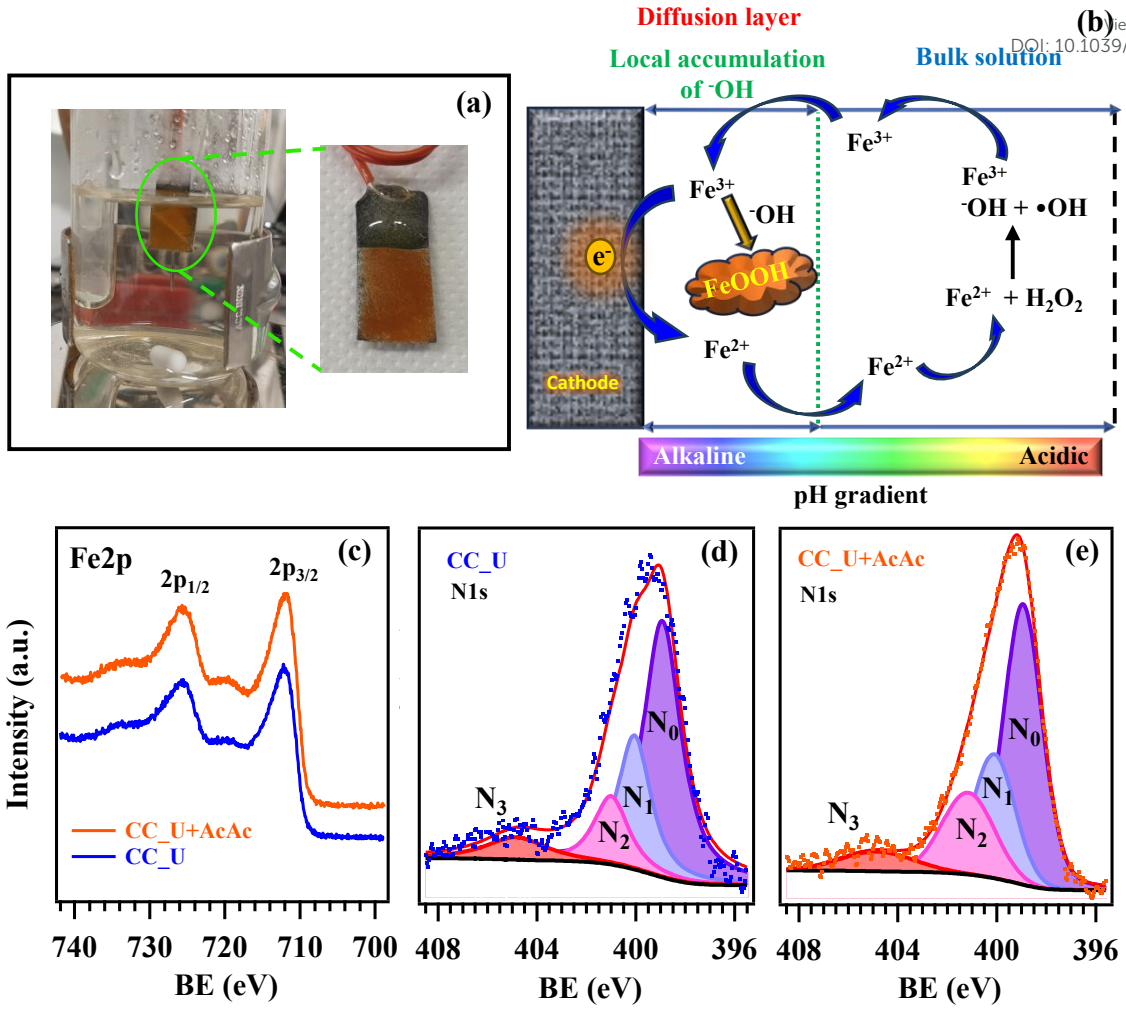

Fig. 8 (a) Image of CC_U+AcAc sample after test for 24 h as working electrode in EF processes for FNT degradation. (b) Sketch of the route yielding insoluble Fe(III) deposits onto the electrode's surface. XPS signals after EF tests for Fe2p (c) and N1s (d,e).

in proximity of the electrode surface, promoting thus its precipitation[48] (Fig. 8b). This phenomenon explains why the formation of the observed deposits occurred only on the working electrodes external region during EF tests. However, P2p and S2p BEs were also consistent with the presence of Fe(III) phosphate and sulphate[30] (ESI†, pages S19-S20), besides FeOOH. C1s signals (ESI†, Fig. S14†) pointed out to the presence of C-OH, C-O-C, esters, and carboxylic acids,[31, 47] resulting from the partial oxidation of exposed CC supports and the adsorption of FNT degradation products. Nevertheless, N1s signals (Fig. 8d-e) did not undergo dramatic variations in comparison to the pristine materials (Fig. 2c and S4b†), evidencing that the formation of iron-containing deposits did not induce significant alterations of the underlying gCN.

4. Conclusions

In summary, this work was dedicated to the fabrication and defect engineering of graphitic carbon nitride photoelectrocatalysts for FNT decomposition. The target systems were immobilized on flexible carbon cloths *via* EPD, starting from carbon nitride powders obtained from urea as such either mixed with AcAc. A thorough multi-technique investigation enabled to investigate the interplay between processing conditions and the resulting system physico-chemical and functional properties. In a nutshell, AcAc functionalization promoted gCN adhesion to the substrate, resulting in a more homogeneous distribution of carbon nitride aggregates. The obtained results demonstrated the successful development of gCN supported systems, whose reactivity towards FNT degradation was mainly improved through defect engineering thanks to a suppressed electron-hole recombination.

EF tests allowed to confirm the remarkable electrochemical stability of the present electrocatalysts, an important starting point for practical applications. Material characterization after degradation tests highlighted the formation of insoluble Fe-containing species on the electrode surfaces, which, however, did not result in an appreciable performance decrease and in alterations of the underlying carbon nitride. The obtained results, which, to the best of our knowledge, have no literature precedents up to date, open challenging perspectives for the implementation of electro-Fenton technique and the subsequent scale-up of the target technology in view of real-world water purification activated by natural sunlight. In addition, more detailed studies on the formation mechanisms and the potential toxicological effects of FNT-derived

products represent important issues for future research developments beyond the present study.

Author Contributions

Giacomo Marchiori: investigation, data-curation, formal analysis, writing-original draft. **Roberta Seraglia:** investigation, data curation, writing-original draft. **Gian Andrea Rizzi:** methodology, conceptualization, writing-review and editing. **Chiara Maccato:** methodology, conceptualization, supervision, resources, investigation, writing-original draft. **Mattia Benedet:** investigation, data-curation, formal analysis. **Emanuela Callone** and **Sandra Dirè:** investigation, data curation, writing-reviewing and editing. **Alberto Gasparotto:** investigation, data curation, writing-reviewing and editing. **Davide Barreca:** supervision, resources, investigation, data curation, formal analysis, writing-reviewing and editing.

Conflicts of interest

There are no conflicts to declare.

Acknowledgements

This research was supported by the National Council of Research (Progetti di Ricerca @CNR-avviso 2020-ASSIST), Padova University (P-DiSC#04BIRD2020-UNIPD EUREKA, P-DiSC#02BIRD2023-UNIPD RIGENERA, DOR 2021–2024), INSTM Consortium (INSTM21PDGASPAROTTO-NANO^{MAT}, INSTM21PDBARMAC-ATENA), and PRIN 2022474YE8 SCI-TROPHY project, financed by the European Union - Next Generation EU - Bando PRIN 2022 – M4.C2.1.1

References

1 L. G. Sultatos, *J. Toxicol. Environ. Health*, 1994, **43**, 271-289.
2 T. O. Ajiboye, P. O. Oladoye, C. A. Olanrewaju and G. O. Akinsola, *Environ. Nanotechnol. Monit. Manage.*, 2022, **17**, 100655.
3 I. A. Saleh, N. Zouari and M. A. Al-Ghouti, *Environ. Technol. Innovation*, 2020, **19**, 101026.
4 H. Mali, C. Shah, B. H. Raghunandan, A. S. Prajapati, D. H. Patel, U. Trivedi and R. B. Subramanian, *J. Environ. Sci.*, 2023, **127**, 234-250.
5 Y. Deng and R. Zhao, *Curr. Pollut. Rep.*, 2015, **1**, 167-176.
6 E. Brillas, I. Sirés and M. A. Oturan, *Chem. Rev.*, 2009, **109**, 6570-6631.
7 C. Hu, Y. Xiao, Y. Zou and L. Dai, *Electrochem. Energy Rev.*, 2018, **1**, 84-112.
8 X. Lyu, W.-N. Zhang, G. Li, B.-W. Shi, Y.-N. Zhang, H. Chen, S.-C. Li and X. Wang, *ACS Appl. Nano Mater.*, 2020, **3**, 8586-8591.
9 F. K. Kessler, Y. Zheng, D. Schwarz, C. Merschjann, W. Schnick, X. Wang and M. J. Bojdys, *Nat. Rev. Mater.*, 2017, **2**.
10 W. J. Ong, L. L. Tan, Y. H. Ng, S. T. Yong and S. P. Chai, *Chem. Rev.*, 2016, **116**, 7159-7329.
11 L. Chen and J. Song, *Adv. Funct. Mater.*, 2017, **27**.
12 J. Lin, Z. Pan and X. Wang, *ACS Sustainable Chem. Eng.*, 2013, **2**, 353-358.
13 H. Hou, X. Zeng and X. Zhang, *Angew. Chem. Int. Ed.*, 2020, **59**, 17356-17376.
14 W. Niu and Y. Yang, *ACS Energy Lett.*, 2018, **3**, 2796-2815.
15 B. Kalinic, L. Girardi, P. Ragonese, A. Faramawy, G. Mattei, M. Frasconi, R. Baretta, S. Bogialli, M. Roverso, G. A. Rizzi and C. Maurizio, *Appl. Surf. Sci.*, 2022, **596**, 153552.
16 Y. Yang, G. Zeng, D. Huang, C. Zhang, D. He, C. Zhou, W. Wang, W. Xiong, X. Li, B. Li, W. Dong and Y. Zhou, *Appl. Catal., B*, 2020, **272**, 118970.
17 J. Yang, Z. Ji and S. Zhang, *ACS Appl. Energy Mater.*, 2023, **6**, 3401-3412.
18 M. Benedet, G. A. Rizzi, A. Gasparotto, O. I. Lebedev, L. Girardi, C. Maccato and D. Barreca, *Chem. Eng. J.*, 2022, **448**, 137645.
19 M. Benedet, A. Gallo, C. Maccato, G. A. Rizzi, D. Barreca, O. I. Lebedev, E. Modin, R. McGlynn, D. Mariotti and A. Gasparotto, *ACS Appl. Mater. Interfaces*, 2023, **15**, 47368-47380.
20 M. Benedet, G. A. Rizzi, O. I. Lebedev, V. Roddatis, C. Sada, J.-L. Wree, A. Devi, C. Maccato, A. Gasparotto and D. Barreca, *J. Mater. Chem. A*, 2023, **11**, 21595-21609.
21 E. Scattolin, M. Benedet, G. A. Rizzi, A. Gasparotto, O. I. Lebedev, D. Barreca and C. Maccato, *ChemSusChem*, 2024, e202400948.
22 S. Benedoue, M. Benedet, A. Gasparotto, N. Gauquelin, A. Orekhov, J. Verbeeck, R. Seraglia, G. Pagot, G. A. Rizzi, V. Balzano, L. Gavioli, V. D. Noto, D. Barreca and C. Maccato, *Nanomaterials*, 2023, **13**, 1035.
23 M. Benedet, G. Andrea Rizzi, A. Gasparotto, N. Gauquelin, A. Orekhov, J. Verbeeck, C. Maccato and D. Barreca, *Appl. Surf. Sci.*, 2023, **618**, 156652.
24 https://xpspeak.software.informer.com/4.1/.
25 W. Zhang, Q. Zhang, F. Dong and Z. Zhao, *Int. J. Photoenergy*, 2013, **2013**, 1-9.
26 Y. Zheng, Z. Zhang and C. Li, *J. Photochem. Photobiol., A*, 2017, **332**, 32-44.
27 V. Devthade, D. Kulhari and S. S. Umare, *Mater. Today Proc.*, 2018, **5**, 9203-9210.
28 M. Ismael, Y. Wu, D. H. Taffa, P. Bottke and M. Wark, *New J. Chem.*, 2019, **43**, 6909-6920.
29 Y. Hu, Y. Shim, J. Oh, S. Park, S. Park and Y. Ishii, *Chem. Mater.*, 2017, **29**, 5080-5089.
30 https://srdata.nist.gov/xps, accessed October, 2023.
31 I. Bertóti, M. Mohai and K. László, *Carbon*, 2015, **84**, 185-196.
32 M. Benedet, A. Gasparotto, G. A. Rizzi, D. Barreca and C. Maccato, *Surf. Sci. Spectra*, 2022, **29**, 024001.
33 M. Benedet, G. A. Rizzi, D. Barreca, A. Gasparotto and C. Maccato, *Surf. Sci. Spectra*, 2023, **30**, 014004.
34 P. Qiu, C. Xu, H. Chen, F. Jiang, X. Wang, R. Lu and X. Zhang, *Appl. Catal., B*, 2017, **206**, 319-327.
35 P. Qiu, H. Chen and F. Jiang, *RSC Adv.*, 2014, **4**, 39969-39977.
36 T. Ma, J. Bai and C. Li, *Vacuum*, 2017, **145**, 47-54.
37 Y. Fu, C. a. Liu, C. Zhu, H. Wang, Y. Dou, W. Shi, M. Shao, H. Huang, Y. Liu and Z. Kang, *Inorg. Chem. Front.*, 2018, **5**, 1646-1652.
38 X. Wang, J. Meng, X. Zhang, Y. Liu, M. Ren, Y. Yang and Y. Guo, *Adv. Funct. Mater.*, 2021, **31**.
39 L. Cheng, H. Zhang, X. Li, J. Fan and Q. Xiang, *Small*, 2021, **17**, 2005231.
40 X. Zhan, Y. Zhao, Y. Sun, C. Lei, H. Wang and H. Shi, *Chemosphere*, 2022, **307**, 136087.
41 S. Li, G. Dong, R. Hailili, L. Yang, Y. Li, F. Wang, Y. Zeng and C. Wang, *Appl. Catal., B*, 2016, **190**, 26-35.

View Article Online
DOI: 10.1039/D4LF00259H

42 J.-y. Chen, N. Li and L. Zhao, *J. Power Sources*, 2014, **254**, 316-322.
43 E. Brillas and S. Garcia-Segura, *Sep. Purif. Technol.*, 2020, **237**, 116337.
44 M. Kerzhentsev, C. Guillard, J.-M. Herrmann and P. Pichat, *Catal. Today*, 1996, **27**, 215-220.
45 J.-M. Herrmann, *Catal. Today*, 1999, **53**, 115-129.
46 V. Leandri, J. M. Gardner and M. Jonsson, *J. Phys. Chem. C*, 2019, **123**, 6667-6674.
47 J. F. Moulder, W. F. Stickle, P. E. Sobol and K. D. Bomben, *Handbook of X-ray Photoelectron Spectroscopy*, Perkin Elmer Corporation, Eden Prairie, MN, USA, 1992.
48 F. Deng, H. Olvera-Vargas, M. Zhou, S. Qiu, I. Sires and E. Brillas, *Chem. Rev.*, 2023, **123**, 4635-4662.

View Article Online
DOI: 10.1039/D4LF00259H

Data Availability Statement

All the data can be found within the manuscript and ESI† files.